Understanding the nature of atmospheric acid processing of mineral dusts in supplying bioavailable phosphorus to the oceans

Anthony Stockdale[a, 1], Michael D. Krom[a,b], Robert J. G. Mortimer[c], Liane G. Benning[a,d], Ken S. Carslaw[a], Ross J. Herbert[a, 2], Zongbo Shi[e], Stelios Myriokefalitakis[f], Maria Kanakidou[f] and Athanasios Nenes[g,h,i]

[a]School of Earth and Environment, University of Leeds, Leeds, UK

[b]Department of Marine Biology, Haifa University, Israel

[c]School of Animal, Rural and Environmental Sciences, Nottingham Trent University, Nottingham, UK

[d]German Research Center for Geosciences, GFZ, Potsdam, Germany

[e]School of Geography and Earth Sciences, University of Birmingham, Birmingham, UK

[f]Environmental Chemical Processes Laboratory, Department of Chemistry, University of Crete, Greece

[g]Earth & Atmospheric Sciences and Chemical & Biomolecular Engineering, Georgia Institute of Technology, Atlanta, GA, USA

[h]National Observatory of Athens, Athens, Greece

[i]Foundation for Research and Technology Hellas, Patras, Greece

[1]Corresponding author. Email: tony@biogeochemistry.org.uk

Tel: +44113 343 2846

[2]Present address: Department of Meteorology, University of Reading, Reading, UK.

Classification: Physical Sciences: Environmental Sciences

Short Title: Bioavailable phosphorus in atmospheric dust

Abstract

Acidification of airborne dust particles can dramatically increase the amount of bioavailable phosphorus (P) deposited on the surface ocean. Experiments were conducted to simulate atmospheric processes and determine the dissolution behaviour of phosphorus compounds in dust and dust precursor soils. Acid dissolution occurs rapidly (seconds to minutes) and is controlled by the amount of H^+ ions present. For H^+ $<10^{-4}$ mol per gram dust, 1-10% of the total phosphorus is dissolved, largely as a result of dissolution of surface-bound forms. At H^+ $>10^{-4}$ mol per gram of dust, the amount of phosphorus (and Ca) released follows a power law dependent on the amount of H^+ consumed until all inorganic phosphorus minerals are exhausted and the final pH remains acidic. Once dissolved, phosphorus will stay in solution due to slow precipitation kinetics. Dissolution of apatite-P, the major mineral phase in dust (79-96%), occurs whether $CaCO_3$ is present or not, though the increase in dissolved phosphorus is greater if $CaCO_3$ is absent or if the particles are externally mixed. The system was modelled adequately as a simple mixture of apatite-P and calcite. Phosphorus dissolves readily by acid processes in the atmosphere in contrast to iron, which dissolves slower and is subject to re-precipitation at cloud water pH. We show that acidification can increase bioavailable phosphorus deposition over large areas of the globe, and may explain much of the previously observed patterns of variability in leachable phosphorus in oceanic areas where primary productivity is limited by this nutrient (e.g. Mediterranean).

Significance statement

Mineral dust is the most important external source of phosphorus, a key nutrient controlling phytoplankton productivity and carbon uptake, to the offshore ocean. The bioavailable phosphorus in dust exhibits considerable and poorly understood variability. Detailed laboratory experiments elucidate and quantify the major processes controlling phosphorus dissolution in the atmosphere. Dust exposure to acids is the main driver of phosphorus mineral transformations, and a simple power law relationship is found between the amount of bioavailable phosphorus dissolved from the dust and acid exposure. Simulations suggest

that dust acidification increases leachable phosphorus over large areas of the globe and explains much of its variability in important oceanic areas where primary productivity is limited by this nutrient (e.g. N. Central Atlantic and Mediterranean).

Author contributions: A.S., M.D.K., R.J.G.M., K.S.C. and L.G.B designed research; A.S., M.D.K. performed research; A.S., M.D.K., R.J.G.M., L.G.B., K.S.C., R.J.H., Z.S. S.M., M.K. and A.N. analyzed data and developed the modelling; and A.S., M.D.K., R.J.G.M., L.G.B., K.S.C., R.J.H., Z.S. and A.N. wrote the paper.

/body

Introduction

Atmospheric inputs are an important source of externally supplied nutrients to the offshore ocean (1). While all of the inorganic nitrogen is water-soluble and immediately bioavailable, most phosphorus (P) and iron (Fe) is present as minerals that are not immediately soluble in water, hence not bioavailable (2, 3). Such mineral particles, if deposited to the surface ocean, may pass through the photic zone with no effect on primary productivity, owing to their high settling velocity and low solubility (2).

Atmospheric P can be important as the major external supply to the offshore ocean particularly in oligotrophic areas of the open ocean (1) and areas that are P limited such as the Sargasso Sea (4) and Mediterranean (5). The most important source of atmospheric P is desert dust, which has been estimated to supply 83% (1.15 Tg P a^{-1}) of the total global sources of atmospheric phosphorus (6). Of that dust they estimate 10% is as leachable P. However observations suggest that the fraction of leachable P in dust is highly variable (7-100%) (7). Only one global modelling study primitively simulates such variability, considering reaction of protons with apatite minerals using a kinetic approach (8). The same study indicates that deposition of P from biological particles of terrestrial origin may be as important as leachable P from dust over the ocean in some regions and certain seasons. This translates to a large predictive uncertainty of the bioavailable P input to the oceans. Studies show that, whilst atmospheric N and Fe supply are of importance on a global scale, atmospheric P supply plays an important secondary role, especially through co-limitation with either N or Fe (9, 10). The varying demands and resilience of different phytoplankton communities can have feedbacks on local limiting nutrients on relatively short time scales (11, 12). Additionally, evidence suggests feedbacks in the surface waters that may enhance the impact of the atmospheric supply of P (1, 13). This complex picture is yet to be replicated in global biogeochemistry models and therefore it is not currently possible to put a limit on the importance of any atmospherically supplied P.

Previous studies have shown that atmospheric processes can increase Fe bioavailability in dust before being deposited to the ocean. Insoluble Fe, principally as iron oxides, can be solubilised by, interaction with acid gases that reduce the pH of atmospheric water to the level where solid phase Fe species can start to dissolve (14), by interaction with organic ligands or by UV photoreduction at predicted considerable amounts (15). By contrast, the principal mineral species of P in aerosols, apatite minerals (e.g., hydroxyapatite, $Ca_5OH(PO_4)_3$), are only expected to be solubilised by acid processes in the atmosphere since they do not undergo photoreduction and Ca is not strongly complexed by organic ligands. Nenes et al. (7) in a study on dust particles sampled in the eastern Mediterranean, found a correlation between increased leachable inorganic phosphorus (LIP) and increased acid exposure in the aerosol particles. Furthermore, the amounts of P released during acidification were consistent with the thermodynamic limit of solubility. However, no further insight on the mechanism and dissolution kinetics could be obtained.

The principal acid precursor species in the atmosphere are NO_X and SO_X. These can be the result of natural processes such as the oxidation of dimethyl sulphide (DMS) released by phytoplankton in oceanic surface waters (16), volcanic eruptions (17), or lightning. However, at present the main source of such gases is anthropogenic (18). To a lesser degree, low molecular-weight carboxylic acids (such as formic, acetic, and oxalic) are generated in large amounts in the atmosphere and can contribute acidity, especially in evaporated cloud droplets (18, 19).

Fresh and aged dust particles can be contained within cloud droplets that dissolve acidic gases but with pH levels that do not drop much below 4 (18). Although some cloud droplets condense to form rain, most cloud droplets evaporate to form wet aerosol particles. This process results in a substantial drop in pH and an increase in ionic strength (IS) of the resultant film of water (20). This cycling between cloud droplet and wet aerosol can occur several times (an average of 10 cycles throughout the troposphere (18)) before the aerosol

drops to earth by wet or dry deposition. Thus the chemical conditions within and between clouds are very different, with relatively high pH and low IS in cloud droplets and low pH and high IS in wet aerosols (20-22). This cycling was investigated for its effect on Fe dissolution in the atmosphere by Shi et al. (23) who show that Fe is solubilised in wet aerosols and then re-precipitated as Fe nanoparticles in clouds. By contrast, the impact of pH changes or proton addition to atmospherically processed mineral dusts and subsequent P dissolution is virtually unknown (see also SI.1.2.).

This study sets out to investigate the nature, magnitude and controls of atmospheric acid processes on the solubilisation of mineral P in dust particles using samples collected during dust storms in Israel and Greece, and on dust precursors collected from surface soils in a variety of locations across the Sahara desert (map included in the supporting information, SI.F1.1.). Experiments were carried out using principally natural dust particles to mimic atmospherically relevant conditions and thereby represent the amount of P solubilised by atmospheric acid processes. Results are interpreted by modelling the experimental systems using the geochemical PHREEQC model (24). Calculations using a global 3-D atmospheric chemical transport model (TM4-ECPL; 25) were used to estimate the potential global importance of these processes.

Results

Properties of dusts. The highest P concentration was found in the dust sample from Israel (Fig. 1 top panel). The sequential phosphate extractions (SEDEX; 26) revealed that apatite was the dominant P mineral (Fig. 1, bottom panel). Total inorganic P (which includes leachable P, iron bound P, apatite P, and carbonate P) varied between 7.7 and 60.0 μmol g^{-1}, and represents 55 to 92% of the total SEDEX phosphorus in the sample. The remainder of the phosphorus was made up of organic P (for full SEDEX data, mineral composition and BET surface area see SI.3.1.2.).

Effect of protons and fluid volume on the dissolution of Ca and P minerals. Fig. 2 shows the combined effects of pH and volume on the release of phosphorus from the Israel dust (legends used in this Figure are used consistently in all subsequent Figures and within the *Supporting Information*). Both more acid pH values (at equal water volume) and higher volumes (at equal pH) yield greater P concentrations. The amount of P (Fig. 2 and 3) and Ca (Fig. 4) released from the dust was controlled by the amount of H^+ ions present and not the initial pH. Fig. 3 shows the released P plotted versus the absolute concentration of protons in the experiments (i.e., mol of H^+ per g of dust). The data showed that below a critical proton concentration of ~0.1 mmol per gram of dust (-4 log mol(H^+)/g dust), the released P was only affected by water volume and not the proton concentration. Above this proton concentration, an approximately linear increase in P with increasing initial proton concentration was seen, until a plateau was reached (~-2.1 log mol(H^+)/g dust), where the acid reactive mineral phosphate pool was exhausted. A similar pattern was seen with Ca (Fig. 4), although the critical proton concentration was slightly lower than that seen for P. These Figures indicate that above a given proton concentration, both Ca and P mineral phases are subject to dissolution. Fe was only above the detection limits in limited experiments where excess protons allowed the pH to remain low throughout the experiment. Results for the other dust samples yielded similar trends for all analytes (see SI.3.2.).

In all experiments the dust-solution mixtures tended to become buffered to neutral or alkali pH end-points after 48 hr of reaction. The exceptions were experiments where protons remained in excess and all Ca and P minerals were dissolved (SI.3.2.1.). Even using buffered solutions (SI.3.1.1.) the release profiles for P did not change from those described above. Similarly, instantaneous acid addition or slow acid diffusion also did not significantly alter the evolution of dissolved P in the experiments (SI.3.2.2.). When we tested a sequential batch addition of acid, the results (Fig. 3, 1 mL experimental data connected by solid line; see also SI.3.2.3.) were similar to experiments performed at higher concentration through a

177 single acid addition, implying consistent Ca and P mineral dissolution as the total proton
178 exposure is increased. Finally, high IS also played a minimal role in driving P release
179 (SI.3.2.3.).
180
181 All experiments with the real dusts described above assumed that the reactive minerals
182 (calcite and apatite) are found in every particle ("internally mixed") at the ratio that can be
183 calculated from the apatite and calcium concentrations determined in our study (Table
184 SI.T3.1.). Although dust particles may be in reality "externally mixed" (particles of a given
185 size have only calcite or apatite but not both), the low volume experiments brought the acidic
186 fluid in contact with all particles, and thus the system behaved as internally mixed. $CaCO_3$
187 controlled the H^+ content and the released phosphorus was totally dependent on reactive
188 mineral composition. These results were confirmed experimentally through analogue dusts
189 made up of single reactive mineral components (i.e., apatite only) or mixed reactive mineral
190 components (apatite and calcite) that we used as dust proxies (SI.3.2.4.). The analogue
191 experiments demonstrate that if dust particles were externally mixed then there would have
192 been more P released per H^+ amount compared to our real dust experiments (Fig. 2 and 3)
193 because more protons are available for direct reaction with apatite.
194
195 **Comparison of experimental results with modelling.** The close agreement between our
196 precursor and real dust samples (SI.3.2.4.) suggests that the interaction between calcite and
197 apatite with acidity, is the primary control of P solubility. This is confirmed by thermodynamic
198 calculations for a system containing only calcite, apatite and solution (Fig. 5 and SI.3.3.).
199 Above approximately 10^{-6} mol L^{-1} for P and 10^{-4} mol L^{-1} for Ca there was agreement
200 between measurements and predictions. Below these concentrations, predicted Ca and P
201 deviated somewhat from the measurements; likely owing to desorption of loosely bound P
202 (SEDEX sorbed pool, Fig. 1, SI.T3.1.) and Ca.
203
204 **Discussion**

205 We studied the dissolution of P-containing phases in the surface soils from areas that are
206 known to be sources of Saharan dust (27) as well as two samples of dry deposited
207 Saharan/Arabian dust. There was a relatively constant P speciation in the mineral
208 composition of these dusts (Fig. 1). Given that the principal acid soluble mineral apatite-P
209 (Ap-P), was on average 89 ± 7 % of the total inorganic P and Fe bound-P was only 7 ± 4%
210 of the acid reactive mineral phases, we consider the proton reactions of only Ap-P and
211 $CaCO_3$ as controlling the atmospheric conversion of mineral P to leachable forms. Other
212 processes that affect the solubilisation of Fe, such as photoreduction and organic
213 complexation (12), are likely to have a minor role in increasing P bioavailability because only
214 Fe bound-P will be affected by such processes. There is no evidence of organic P being
215 affected by acidification. In addition to these acid soluble phases, a small amount (< 7%)
216 was in the sorbed inorganic-P pool (extracted by 1M $MgCl_2$), which is likely to be solubilised
217 directly into seawater (26).
218
219 Although our samples were collected or derived from widespread areas from the Sahara and
220 Arabian deserts, they all had similar relative fractions of Ap-P, Fe-bound-P and adsorbed-P.
221 This is consistent with a common weathering regime across these deserts, which combines
222 some chemical weathering, little plant growth to convert P minerals into plant biomass in-situ
223 and often reprecipitation of $CaCO_3$ as caliche. However, we recognise that other regions of
224 the Sahara, with different mineralogy (e.g. the Bodélé (28)), may exert an influence on the
225 bulk properties of some Sahara dust plumes. Our samples had 7×10^{-4} to 3.3×10^{-3} mol g^{-1}
226 acid soluble Ca, which is 6-33% by mass of $CaCO_3$. Although the P mineral speciation was
227 similar between samples, there was considerable variability in the total P concentration (9.1
228 $\times 10^{-6}$ to 6.3×10^{-5} mol g^{-1}).
229
230 In the atmosphere, dust particles cycle between clouds where they can become cloud
231 condensation nuclei and wet aerosols. In clouds there is a high water:dust ratio, low IS and

generally high pH except in the unusual situation of very highly polluted air masses. Wet aerosols, which are generally formed when cloud water evaporates, contain a film of water and can have very low water:dust ratios, high IS and low pH (23). Our experiments were designed to span these conditions within the practical limitations of laboratory handling. The key parameter in controlling the amount of P (and Ca) liberated from acid processing was the total amount of H^+ ions in the aqueous layer surrounding the dust particle and not the initial pH (Fig. 2-4). For all of our experiments, both $CaCO_3$ and Ap-P were rapidly dissolved (as measured by Ca^{2+} and PO_4-P liberated) and H^+ ions consumed, on a timescale of second to minutes (SD3.1.1.). In most cases the pH was controlled by rapid reaction with $CaCO_3$ to circumneutral values as shown by the simple relationship between the decrease in H^+ ions being twice the increase in Ca^{2+} cations.

At low H^+ amounts (< 10^{-4} mol g^{-1} dust) P was liberated over a wide range of H^+ ion concentrations. This was interpreted as being due mainly to simple leaching of dissolved P from the samples into water, independent of the reaction of H^+ with acid soluble minerals. This corresponds to the leachable P previously measured when dust was treated by deionised water or a very low strength leach (e.g. (29)). The amount of leached P is likely to be independent of whether there is $CaCO_3$ in the dust sample or not.

At proton concentrations above 10^{-4} mol H^+ per gram of dust, there was a power law relationship between P (and Ca) released and the amount of H^+ ions consumed (Fig. 2-4). This relatively simple pattern of P release continued until the level where all of the P minerals were exhausted. This was also the value at which the final pH in solution was no longer circumneutral but remained acidic. This value corresponded approximately to the value of total inorganic P determined by SEDEX extraction. Similar trends were obtained for all the other dust and dust precursor samples.

259 The relationship between P, Ca^{2+} and H^+ ions for all the test samples was confirmed by
260 PHREEQC equilibrium modelling in which there were similar increasing trends of P and Ca^{2+}
261 obtained assuming a simple 3-component model of calcite, hydroxyapatite and H^+ ions. The
262 model fit was better for Ca^{2+} (controlled by calcite and H^+ ions) than P where there was more
263 scatter. This is considered reasonable as there is more than one acid-soluble P mineral
264 present in all the natural samples and the Ap-P is also likely to be made up from a number of
265 different apatite minerals with different solubility behaviour.
266
267 Our results also showed that increased IS caused slightly more dissolved phosphate to be
268 liberated into solution. Where the major contributor to increased IS was ammonium and
269 sulphate, the most common ionic species in aerosols (18), it was found that the amount of P
270 released fits on the trend for the HCl-only data if the proton availability from the dissociation
271 of ammonium ions (predicted from a final pH of 8) is allowed for. In our experiments using
272 NaCl (IS = 2), which was used as a surrogate for evaporated sea salt, the liberated P
273 increased by a factor of 4.3. In both cases even if the IS decreases to that of rainwater the
274 dissolved P will remain in solution due to very slow precipitation kinetics and will be
275 delivered as bioavailable P to the surface ocean (30 and references therein).
276
277 In the atmosphere some mineral particles have both $CaCO_3$ and Ap-P on the same particle
278 (internally mixed) while other particles have only one or the other mineral (externally mixed).
279 Because acidity in the atmosphere is transferred to dust via the gas phase, the amount of
280 dissolved P will vary between particles, depending on the amount of $CaCO_3$. There were no
281 data available characterising the degree of external mixing of $CaCO_3$ and Ap-P in dust
282 samples. However, we expect many of the particles to contain both $CaCO_3$ and Ap-P
283 because in many sedimentary rocks and desert soil systems there is a close association
284 between $CaCO_3$ and Ap-P. Both minerals precipitate in marine sediments during diagenesis
285 (31) and such marine sediments are generally the source of Ap-P in desert soils (32).
286 Furthermore, caliche forms in many desert soils as Ca and bicarbonate produced by in-situ

287 weathering are precipitated (33). However, our results show that in the situation where
288 external mixing does occur, more P would be solubilised because on those particles with
289 only Ap-P, there was no consumption of H^+ by $CaCO_3$ because it was absent from this
290 experiment (Fig. SI.F3.3.). In reality, although we predict that many dust particles will be
291 internally mixed, there will be a continuum and the balance between these two extremes
292 may not be the same for all dust events.
293
294 **Comparison with Fe processes.** The fraction of bioavailable Fe supplied to the ocean is
295 also increased by acidic atmospheric processes (34). However, Fe dissolution is much
296 slower than Ap-P (35). This means that for internally mixed particles, essentially all the H^+
297 ions will be neutralised by $CaCO_3$ before they react with Fe minerals. However Fe-bearing
298 particles are often externally mixed as clays (36) or Fe-rich particles (37). Thus, dissolution
299 of Fe and P can happen simultaneously on different particles. Furthermore, Fe dissolution
300 occurs principally in wet aerosols (low pH with high IS; 23). When the aerosol particles are
301 activated into clouds at lower pH, the Fe is likely to re-precipitate as nanoparticles (38) while
302 P does not re-precipitate. The only removal of P will be adsorption onto fresh Fe
303 nanoparticles if both processes occur on the same particle/droplet. In that situation both Fe
304 and sorbed P are likely to be bioavailable.
305
306 **The potential importance to the global P cycle and supply to the ocean.** The main acids
307 in the atmosphere, H_2SO_4 and HNO_3, are generated by the oxidation of sulphur and nitrogen
308 gases emitted by biogenic, volcanic and anthropogenic sources (16-18), the latter of which is
309 dominant at present. It has been noted that there is a higher fraction of LIP in polluted air
310 masses (39, 40). Based on field samples collected in Crete, Nenes et al. (7) provided direct
311 evidence of the increase in LIP in aerosols with increasing aerosol acidity. They suggest that
312 this is from polluted air masses from southern Europe bringing acid gases from the north to
313 mix with Saharan air mass. The increased fraction of LIP in atmospheric aerosols over the
314 Bay of Bengal compared to those over the Arabian Sea, has also been interpreted as due to

315 the effect of acid processing of aerosols caused by anthropogenic activities (41). The action
316 of the processes identified here may explain why aerosol samples across the N central
317 Atlantic can have greater fractions of soluble P than dust soil precursors or aerosols
318 collected closer to the dust source (42). Our results demonstrate that atmospheric acid
319 processes are extremely efficient in solubilising P and provide further support to Nenes et al.
320 (7) that acids can increase the delivery of bioavailable P from dust to the oceans. The
321 amount of N fixation is also likely to increase since dust that has been acid processed will
322 contain increased amounts of both bioavailable P and Fe which have been shown to limit N
323 fixation (9).
324
325 To examine whether acid dissolution of dust P can be globally important, we simulate the
326 acid exposure of dust, and examine the extent to which it can occur. For this, we quantify the
327 ratio between dust Ca and its acid exposure. We quantify the ion balance, $I_b = 2[SO_4] +$
328 $[NO_3] + [Cl] - 2[Ca] - [NH_4] - [Na] - 2[Mg] - [K]$ (where [X] represents the concentration of
329 species X in the aerosol sample, in mol m^{-3} air) over aerosol Ca (Fig. 6). Calculations are
330 carried out with the global model framework of Myriokefalitakis et al. (25) using current day
331 aerosol emissions and results are shown for coarse fraction of dust and the model surface
332 layer, which is representative of the dust that deposits to the surface. Values of the ratio
333 above 10^{-1} indicate regions where considerable solubilization of dust P is expected. The
334 simulations clearly indicate that the flux of bioavailable P over considerable regions of the
335 ocean can be substantially increased by acidified dust. This increase is likely to be greater
336 than the 0.53 Tmol C yr^{-1} that can be calculated from the predicted P solubilised by the
337 kinetic apatite-P dissolution process presented in recent global modelling work (8).
338
339 In many locations there has been a greater increase in N containing gases (particularly NO_x
340 and NH_3) than particulate P, which is transported in the atmosphere. The molar ratio is
341 typically greater than 16:1 and often much larger. It has been reported that this supply tends
342 to make surface waters more P limited (43, 44). Our results suggest that this transformation

343 is somewhat moderated by the relative increase in bioavailable P due to interaction between
344 NO_x and dust particles. As a result, phytoplankton biomass and carbon uptake will increase
345 even in areas of the ocean which are N limited in the short term since P remains the element
346 which causes longer-term increase in primary productivity (45). The implications of this
347 added carbon export from anthropogenic pollution to ocean ecosystems has the potential to
348 be widespread and considerable, affecting global primary productivity and the carbon cycle.
349
350 **Methods**
351 **Dust and precursor dust sources.** Two dust samples and six size fractionated dust
352 precursor samples were used in this study (Table 1). The majority of the experiments were
353 carried out with a dust sample deposited on a clean, flat surface during a dust storm in Rosh
354 Pina, Israel (collected 1st May 2012). A second dust sample was collected between June 1st
355 and 9th, 2013 from a solar panel in Heraklion (Crete, Greece). Based on back trajectory data
356 from the HYSPLIT model (http://ready.arl.noaa.gov/HYSPLIT.php), the origins of these dusts
357 were the deserts of Saudi Arabia/Jordan/Iraq, and North Africa, respectively. These two real
358 dusts were used directly as collected, without size fractioning or other pre-conditioning. In
359 addition, six dust precursor samples collected from a variety of locations (mainly dry stream
360 or lake bed soils) within the Sahara Desert (Table 1) were used to generate size fractionated
361 dusts using a dust tower separation and filtration methods (46). We used the <10 μm
362 (PM10) fractions for our experiments, similar to previously used dust precursors that have
363 been shown to be analogous to atmospherically sampled dust (46, 47). In this present study
364 the term dust is used to refer to both the dust precursor and the real dust samples unless
365 otherwise stated.
366
367
368 **Experimental procedures.** *SEDEX sequential phosphorus extraction.* Phosphorus
369 speciation amongst the different operationally-defined P pools was determined on 50-100
370 mg of each dust (Table 1) following the SPExMan SEDEX sequential extraction scheme

371 (48), with the modification that step IIA for Fe bound P followed the procedure of (49). This
372 modification removes the use of citrate, slightly alters the pH to 7.5 and increases the
373 reaction time to ten hours. The absence of citrate means that the resulting solutions do not
374 require any pre-treatment, other than dilution, before analysis by the molybdate blue method
375 (see below). Five P species were differentiated, namely: leachable or loosely sorbed; Fe
376 bound; a combined pool containing authigenic apatite, biogenic apatite and $CaCO_3$ bound;
377 detrital apatite plus other inorganic P, and organic P. We defined apatite (Ap-P) as the
378 combined phases extracted as diagenetic and detrital apatite, and $CaCO_3$ bound-P in the
379 sequential SEDEX extraction scheme. Total Inorganic P was defined as the sum of all the
380 phases except organic P. Methods for mineral composition and surface area analysis are in
381 SI.2.2.
382
383 *Phosphorous release experiments.* The following experiments were performed on the dust
384 samples using pH adjusted but unbuffered solutions (HCl, Sigma-Aldrich ≥37% ACS reagent
385 grade in 18.2 MΩ·cm MQ water) in an end-over-end stirrer for 48 hours. Israel dust (55±3
386 mg); pH 2 HCl with volumes 70, 140, 210, 500 μL & 1, 2, 5, 15 mL; 0.2 mL HCl at pH 0, 1, 2,
387 3, 4, 5.5; 1 mL HCl at pH 0, 1, 3, 4, 5.5; 2 mL HCl at pH 0.3, 1.3, 2.3, 3.3, 4.3, 5.5; and 5 mL
388 HCl at pH 1, 3, 5.5. Other dusts (30±1 mg); used 1.2 mL at pH 0, 1, 1.8, 2.4. Several initial
389 experiments were carried out to determine the pH buffering capacities and the proton-dust
390 reaction rates. We showed that almost all protons were consumed within ~ 200 seconds of
391 starting the reaction and that the phosphate release was equally fast regardless of initial pH
392 (SD2.2.1. and SI.3.1.1.). Nevertheless, we performed the majority of our experiments over a
393 conservative time period of 48 hours, by which time all changes in concentration had been
394 completed. At the end of these experiments, the mixture was passed through a 0.45 μm
395 syringe filter (13 mm Whatman Puradisc polyethersulfone) and dissolved phosphate was
396 determined as described below. In the experiments with solution volumes ≥ 2 mL the final
397 pH was measured following the 48 hr exposures. The effect of high ionic strength was tested

by adding either ammonium sulphate or NaCl to reach IS = 2 (SI.2.2.2). Furthermore, additional experiments were carried out to evaluate the effect of sequential solution addition (SI.2.2.3.), the effect of acid addition via dialysis (SI.2.2.4.), and the behaviour of simple lab prepared dust analogues (SI.2.2.5.).

Chemical analysis of supernatants. Dissolved inorganic phosphorus was analysed using the molybdate blue reaction (50) after suitable dilution with matrix-matched standards on a segmented flow analyser. For high concentrations (>50 nmoles L^{-1}) this was done on a SEAL Analytical AA3. The RSD was 2.2% (n=8) and limit of detection (LOD; 3 × s.d of blank) was 12 nmoles L^{-1}. Lower concentration samples were analysed using a 100 cm WPI Liquid Waveguide Capillary Cell coupled to an Ocean Optics USB2000+ spectrophotometer with a precision (n=6 of 60 nmoles L^{-1} samples) of 1.6% and a LOD of 2 nmoles L^{-1}. Dissolved calcium and iron concentrations in the supernatants were measured using a Thermo Scientific iCAP 7400 Radial ICP-OES. The Ca and Fe detection limits were <0.1 nmoles and 500 nmoles L^{-1} respectively; with RSD of 1.5% and 1.8% respectively (based on 8 replicates of a 13 mmol L^{-1} (Ca) or 9.0 µmol L^{-1} (Fe) standard). Finally, pH was measured with a Mettler Toledo Seven Excellence meter coupled to an Inlab Expert Pro-ISM pH electrode calibrated with three NIST traceable standard buffers (pH 4, 7 and 9.2; Mettler Toledo).

Geochemical modelling of experimental systems. In order to evaluate the experimental results in terms of predicted equilibrium results, we used the geochemical modelling code PHREEQC (24), with the Lawrence Livermore National Laboratory database. Input conditions were based on the experimental starting solution conditions and assuming only hydroxyapatite and calcite were the reactive minerals present. The relative concentrations of these components were based on the dissolved Ca and P concentrations measured in the experiment for each dust under the most acid conditions.

Global 3-D atmospheric chemistry transport modelling using TM4-ECPL. The ratio of I_b ($2[SO_4] + [NO_3] + [Cl] - 2[Ca] - [NH_4] - [Na] - 2[Mg] - [K]$, where [X] represents the concentration of species X in the aerosol sample, in mol m^{-3} air) to Ca at surface has been calculated using model TM4-ECPL (25) that takes into account anthropogenic and natural emissions as described in the supporting information (SI.2.2.6) and uses ECMWF (European Centre for Medium – Range Weather Forecasts) Interim re–analysis project (ERA – Interim) meteorology to drive atmospheric transport. The model uses the ISORROPIA II thermodynamic model (51) to solve the K^+–Ca^{2+}–Mg^{2+}–NH_4^+–Na^+–SO_4^{2-}–NO_3^-–Cl^-–H_2O aerosol system and enables calculation of the aerosol water pH.

Acknowledgements

Funding was provided by Leverhulme Trust entitled "Understanding the delivery of phosphorus nutrient to the oceans" Grant Number RPG 406. We thank N. Mihalopoulos for fruitful discussions and for providing dust samples and N. Drake for providing dust precursor samples. Z.S. acknowledges support from NERC (NE/I021616/1). A.N. acknowledges support from a Cullen-Peck Fellowship and Georgia Power Scholar funds.

References

1. Paytan A, McLaughlin K (2007) The oceanic phosphorus cycle. *Chem Rev* 107(2):563-576.
2. Eijsink LM, Krom MD, Herut B (2000) Speciation and burial flux of phosphorus in the surface sediments of the eastern Mediterranean. *Am J Sci* 300(6):483-503
3. Shi Z, et al (2012) Impacts on iron solubility in the mineral dust by processes in the source region and the atmosphere: A review. *Aeolian Res* 5:21-42.
4. Wu JF, Sunda W, Boyle EA, Karl DM (2000) Phosphate depletion in the western North Atlantic Ocean. *Science* 289(5480):759-762.
5. Krom MD, Brenner S, Kress N, Gordon LI (1991) Phosphorus limitation of primary productivity in the eastern Mediterranean Sea. *Limnol Oceanogr* 36(3):424-432.

6. Mahowald N, et al (2008) Global distribution of atmospheric phosphorus sources, concentrations and deposition rates and anthropogenic impacts. *Global Biogeochem Cy* 22(4):GB4026.
7. Nenes A, et al (2011) Atmospheric acidification of mineral aerosols: A source of bioavailable phosphorus for the oceans. *Atmos Chem Phys* 11:6265-6272.
8. Myriokefalitakis S, Nenes A, Baker AR, Mihalopoulos N, Kanakidou M (2016) Bioavailable atmospheric phosphorous supply to the global ocean: a 3-D global modelling study. *Biogeosci Discuss* doi:10.5194/bg-2016-215
9. Mills MM, Ridame C, Davey M, La Roche J, Geider RJ (2004) Iron and phosphorus co-limit nitrogen fixation in the eastern tropical North Atlantic. *Nature* 429:292-294.
10. Moore CM, et al (2008) Relative influence of nitrogen and phosphorous availability on phytoplankton physiology and productivity in the oligotrophic sub-tropical North Atlantic Ocean. *Limnol Oceanogr* 53:291-305.
11. Ward BA, Dutkiewicz S, Moore CM, Follows MJ (2013) Iron, phosphorus, and nitrogen supply ratios define the biogeography of nitrogen fixation. *Limnol Oceanogr* 58:2059-2075.
12. Moore CM, et al (2013) Processes and patterns of oceanic nutrient limitation. *Nature Geosci* 6:701-710.
13. Van Mooy BAS, et al (2015) Phytoplankton in the ocean use non-phosphorus lipids in response to phosphorus scarcity. *Nature* 458:69-72.
14. Baker AR, Croot PL (2010) Atmospheric and marine controls on aerosol iron solubility in seawater. *Mar Chem* 120(1-4):4-13.
15. Spokes JL, Jickells TD, Lim B (1994) Solubilisation of aerosol trace metals by cloud processing: A laboratory study. *Geochim Cosmochim Acta* 58(15):3281-3287.
16. Liss PS, Hatton AD, Malin G, Nightingale PD, Turner SM (1997) Marine sulphur emissions. *Philos T Roy Soc Lond B* 352:159-168.
17. Carbonnelle J, Dajlevic D, Zettwoog P, Sabroux JC (1982) Gas output measurements from an active volcano. *Bull Volcanol* 45(3):267-268.
18. Seinfeld JH, Pandis SN (2006) *Atmospheric chemistry and physics; from air pollution to climate change, 2nd Edition*. John Wiley & sons Inc. New York.
19. McNeill VF (2015) Aqueous organic chemistry in the atmosphere: sources and chemical processing of organic aerosols. *Environ Sci Technol* 49(3):1237-1244.
20. Weber RJ, Guo H, Russell AG, Nenes A (2016) High aerosol acidity despite declining atmospheric sulfate concentrations over the past 15 years, *Nat Geosci* 9: 282-285.
21. Meskhidze N, Chameides WL, Nenes A, Chen G (2003) Iron mobilization in mineral dust: Can anthropogenic SO_2 emissions affect ocean productivity? *Geophys Res Lett* 30(21):2085.

22. Zhu X, Prospero JM, Millero FJ, Savoie DL, Brass GW (1992) The solubility of ferric ion in marine mineral aerosol solutions at ambient relative humidities. *Mar Chem* 38(1-2):91-107.
23. Shi Z, Krom MD, Bonneville S, Benning LG (2015) Atmospheric processing outside clouds increases soluble iron in mineral dust. *Environ Sci Technol* 49(3):1472-1427.
24. Parkhurst DL, Appelo CAJ (2013) Description of input and examples for PHREEQC version 3 - A computer program for speciation, batch- reaction, one-dimensional transport, and inverse geochemical calculations: Techniques and Methods, book 6, chap. A43, pp497. U.S. Geological Survey. [http://pubs.usgs.gov/tm/06/a43; accessed 4th May 2015].
25. Myriokefalitakis S, et al (2015) Changes in dissolved iron deposition to the oceans driven by human activity: a 3-D global modelling study. *Biogeosci* 12:3973-3992.
26. Ruttenberg K (1992) Development of a sequential extraction method for different forms of phosphorus in marine sediments. *Limnol Oceanogr* 37(7):1462-1482.
27. Ginoux P, Prospero JM, Gill TE, Hsu NC, Zhao M (2012) Global-scale attribution of anthropogenic and natural dust sources and their emission rates based on MODIS deep blue aerosol products. *Rev Geophys* 50(3):RG3005
28. Hudson-Edwards K, Bristow CS, Cibin G, Mason G, Peacock CL (2014) Solid-phase phosphorus speciation in Saharan Bodélé Depression dusts and source sediments. *Chem Geol* 384:16-26.
29. Baker AR, Kelly SD, Biswas KF, Witt M, Jickells TD (2003) Atmospheric deposition of nutrients to the Atlantic Ocean. *Geophys Res Lett* 30(24):2296.
30. Golubev SV, Pokrovsky OS, Savenko VS (1999) Unseeded precipitation of calcium and magnesium phosphates from modified seawater solutions. *J Cryst Growth* 205(3): 354-360.
31. Van Cappellen P, Berner RA (1991) Fluorapatite crystal growth from modified seawater solutions. *Geochim Cosmochim Acta* 55(5):1219-1234.
32. Gross A, et al (2015) Variability in sources and concentrations of Saharan Dust over the Atlantic Ocean. *Environ Sci Technol Lett* 2(2):31-37.
33. Schlesinger WH (1985) The formation of caliche in soils of the Mojave Desert, California, *Geochim Cosmochim Acta* 49(1):57-66.
34. Meskhidze N, Chameides WL, Nenes A (2005) Dust and pollution: a recipe for enhanced ocean fertilization? *J Geophys Res* 110(D3):D03301.
35. Shi Z, et al (2011) Influence of chemical weathering and aging of iron oxides on the potential iron solubility of Saharan dust during simulated atmospheric processing. *Global Biogeochem Cy* 25, GB2010.

36. Deboudt KA, Mussi GA, Flament P (2012), Red-ox speciation and mixing state of iron in individual African dust particles, *J Geophys Res* 117:D12307.
37. Kandler K, et al. (2009) Size distribution, mass concentration, chemical and mineralogical composition and derived optical parameters of the boundary layer aerosol at Tinfou, Morocco, during SAMUM 2006. *Tellus B* 61(1):32–50.
38. Shi Z, et al. **(**2009) Formation of iron nanoparticles and increase in iron reactivity in the mineral dust during simulated cloud processing. *Environ Sci Technol* 43:6592-6596.
39. Anderson LD, Faul KL, Paytan A (2010) Phosphorus associations in aerosols; What can they tell us about P bioavailability? *Mar Chem* 120(1-4):44-56.
40. Furutani H, Meguro A, Igushi H, Uematsu M (2010) Geographical distribution and sources of phosphorus aerosols over the North Pacific ocean *Geophys Res Lett* 37: L03805.
41. Srinivas B, Sarin MM (2012) Atmospheric pathways of phosphorus to the Bay of Bengal: contribution from anthropogenic sources and mineral dust. *Tellus B*. 64: 17174.
42. Baker AR, Jickells TD, Witta M, Linge KL (2006) Trends in the solubility of iron, aluminium, manganese and phosphorus in aerosol collected over the Atlantic Ocean. *Mar Chem* 98:43-58.
43. Baker AR, Kelly SD, Biswas KF, Witt M, Jickells TD (2003) Atmospheric deposition of nutrients to the Atlantic Ocean. *Geophys Res Lett* 30(24):2296.
44. Christodoulaki S, et al. (2016) Human-Driven Atmospheric Deposition of N and P Controls on the East Mediterranean Marine Ecosystem, *J Atmos Sci* 73(4):1611-1619.
45. Falkowski PG, Barber RT, Smetacek V (1998) Biogeochemical controls and feedbacks on ocean primary production. *Science* 281(5374):200-206.
46. Shi Z, et al (2011) Iron dissolution kinetics of mineral dust at low pH during simulated atmospheric processing. *Atmos Chem Phys* 11(3):995-1007.
47. Lafon S, Sokolik IN, Rajot JL, Caquineau S, Gaudichet A (2006), Characterization of iron oxides in mineral dust aerosols: Implications for light absorption. *J Geophys Res* 111:D21207.
48. Ruttenberg KC, et al (2009) Improved, high-throughput approach for phosphorus speciation in natural sediments via the SEDEX sequential extraction method. *Limnol Oceanogr*: *Methods* 7:319–333.
49. MacDonald KR (2013) Evaluation of selective iron extraction techniques to quantify iron-bound phosphorus in sediments. M.S. Thesis, Department of Oceanography, Univ. of Hawaii.

564 50. Murphy J, Riley JP (1962) A modified single solution method for the determination of
565 phosphate in natural waters. *Anal Chim Acta* 27:31-36.
566 51. Fountoukis C, Nenes A (2007) ISORROPIA II: a computationally efficient
567 thermodynamic equilibrium model for K^+–Ca^{2+}–Mg^{2+}–NH_4^+–Na^+–SO_4^{2-}–NO_3^-–Cl^-–
568 H_2O aerosols. *Atmos Chem Phys* 7(17):4639–4659.
569

Figures

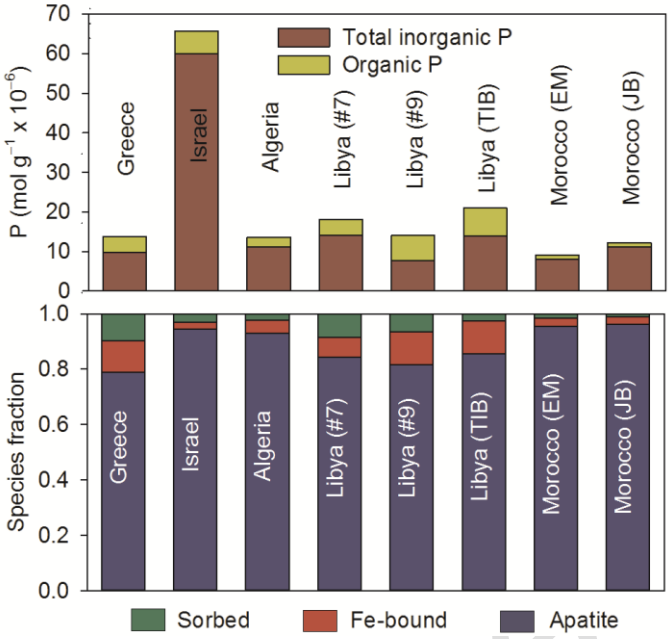

Fig. 1. Phosphorus speciation in the dust and dust precursor samples, as determined by SEDEX. The top panel shows the concentrations of P present in the different samples, the bottom panel details the relative fraction of the different inorganic P species.

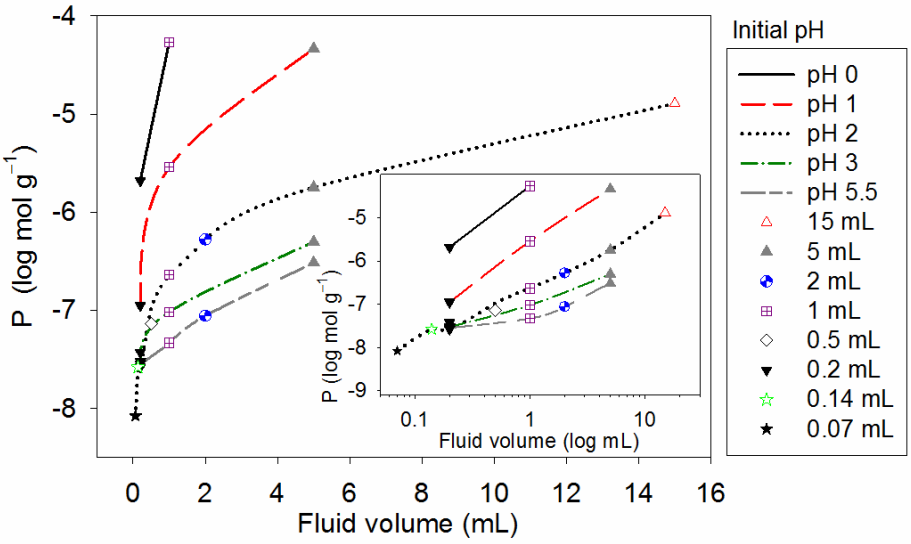

Fig. 2. Dissolved phosphate released from Israel dust in relation to pH and solution volume. Values are presented as moles per gram of dust. Dust masses were ~55 mg, and dust to volume ratios were 3.5 to 704.3 g L^{-1}. Inset panel shows the same data with the volume axis on a log scale.

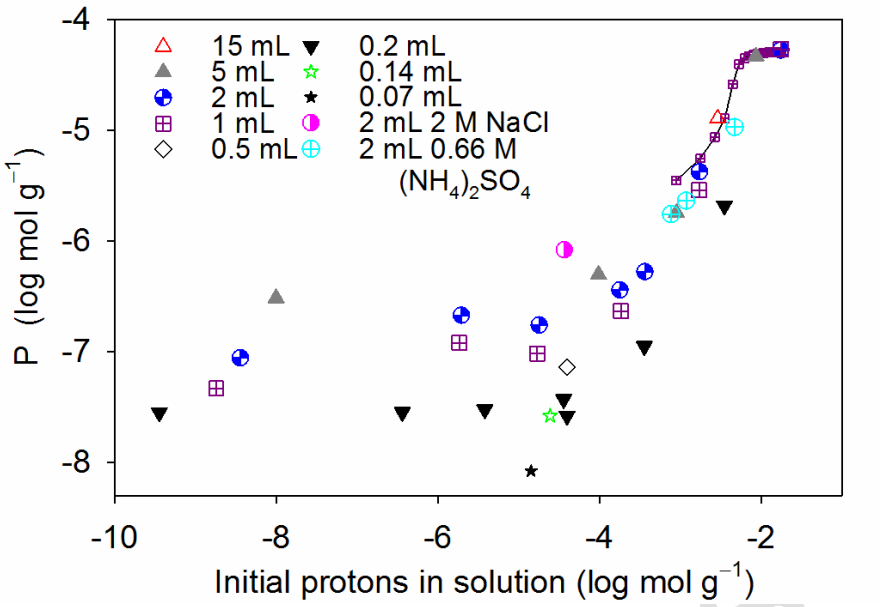

581

582 Fig. 3. Dissolved phosphorus (moles per gram of dust) released from Israel dust in relation
583 to the absolute concentration of protons that were available for reaction at the start of the
584 experiment. Dust masses were ~55 mg, and dust to volume ratios were 3.5 to 704.3 g L^{-1}.
585 The crossed boxes connected by a solid line represent a sequential acid addition experiment
586 (SI.2.2.3.).

587

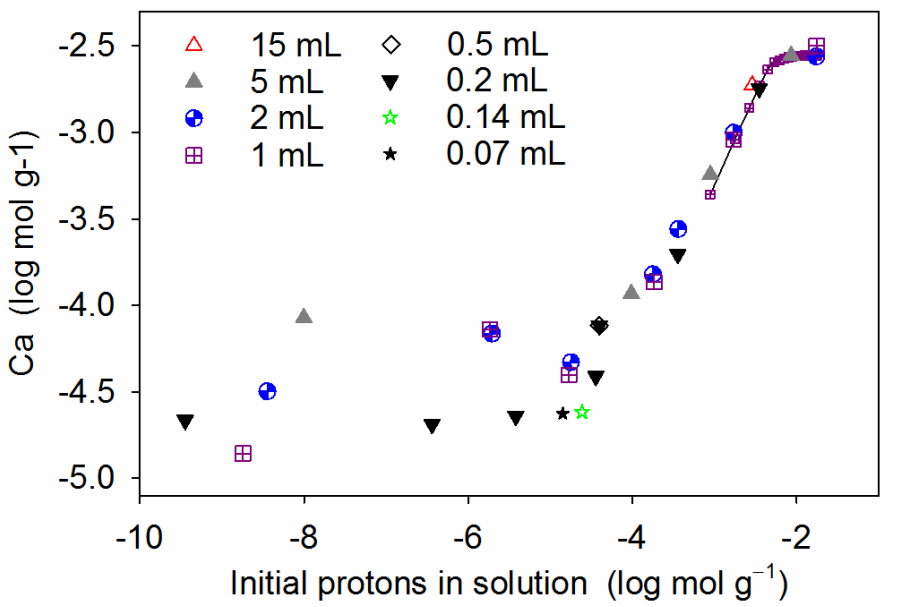

588

589 Fig. 4. Dissolved calcium (moles per gram of dust) released from Israel dust in relation to the
590 absolute concentration of protons that were available for reaction at the start of the
591 experiment. Dust masses were ~55 mg, and dust to volume ratios were 3.5 to 704.3 g L^{-1}.

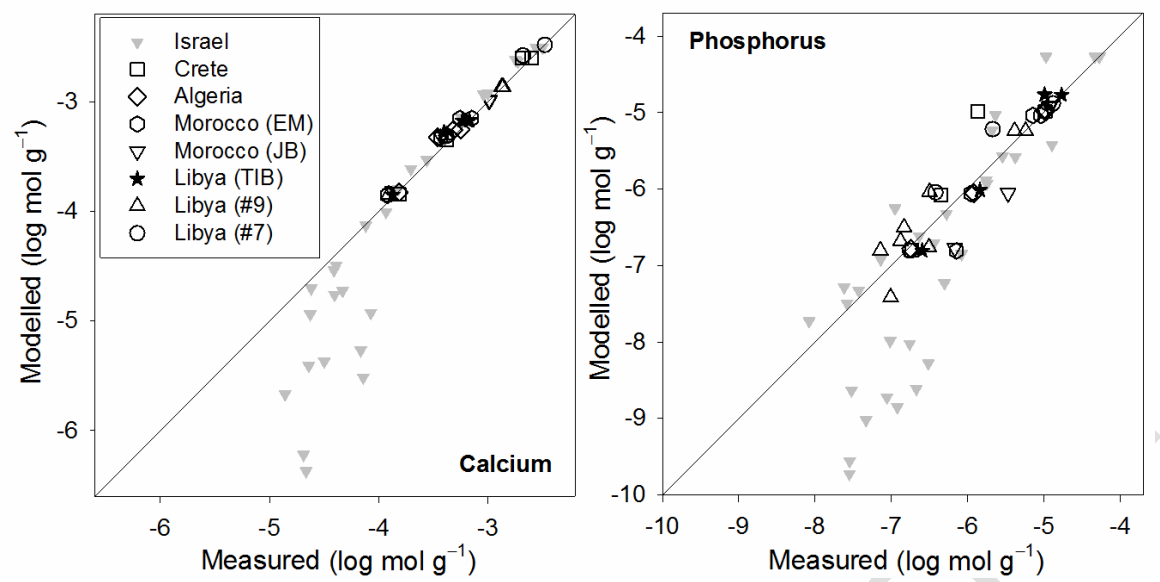

592

593 Fig. 5. Comparison of measured P and Ca dissolution from all dusts compared to equilibrium

594 predictions made using PHREEQC.

595

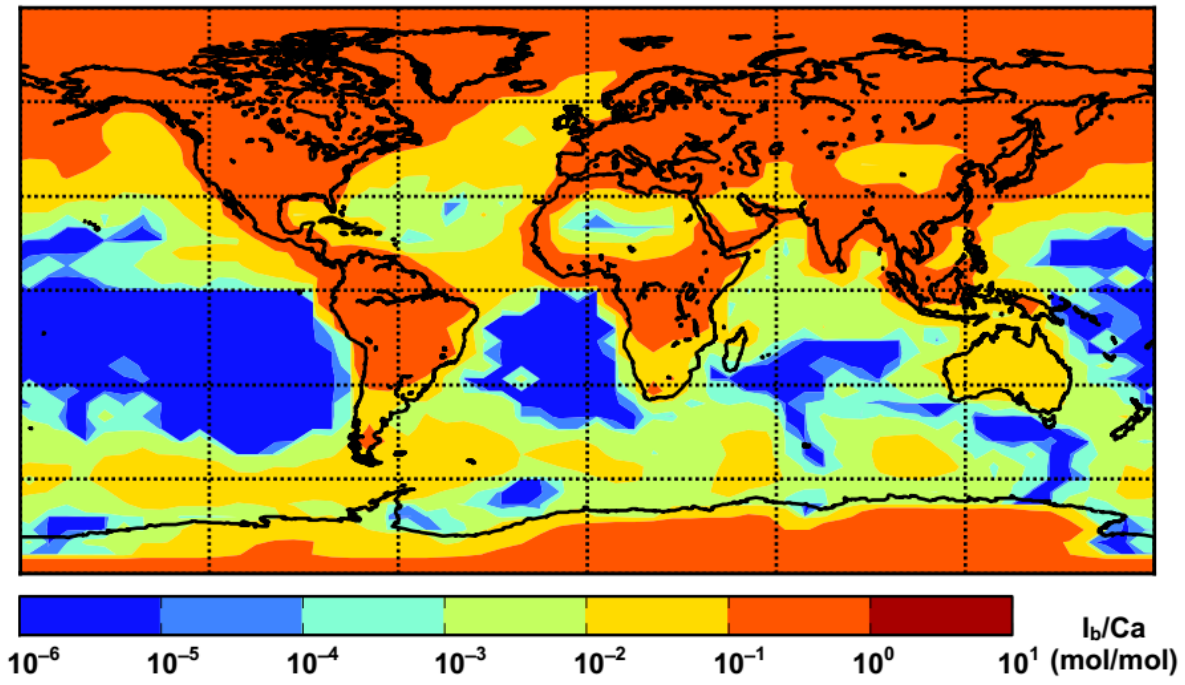

596

597 Fig. 6. Annual average ion balance over aerosol Ca. Calculations are performed with the

598 global model framework of Myriokefalitakis et al. (25) using current day aerosol emissions.

599 Values of the ratio above 10^{-1} indicate regions where considerable solubilization of dust P is

600 expected, presuming that dust aerosol is present.

601

602 **Tables**

603 Table 1. Samples used in this study and their source locations.

Country of origin	Location	Coordinates
Dusts		
Greece	Crete	35°19'51"N, 25°40'04"E
Israel	Rosh Pina	32°58'12"N, 35°33'32"E
Precursor dusts		
Algeria	Bordj Mokhtar (BM)	21°19'30"N, 0°56'46"E
Morocco	El Miyit (EM)	30°21'53"N, 5°37'29"W
Morocco	Jebel Brahim (JB)	29°56'12"N, 5°37'43"W
Libya	#7	32°02'42"N, 22°18'01"E
Libya	#9	32°36'47"N, 22°11'42"E
Libya	Tibesti (TIB)	25°35' N, 16°31' E

604
605